KSME

Springer

Journal of Mechanical Science and Technology 37 (10) 2023

Original Article
DOI 10.1007/s12206-023-0918-3

Keywords:
· Corona discharge
· Computational fluid dynamics
· Dielectric separator
· Electrostatic precipitator

Correspondence to:
Man Yeong Ha
myha@pusan.ac.kr;
Donggeun Lee
donglee@pusan.ac.kr

Citation:
Park, J. H., Ha, M. Y., Lee, D. (2023). A numerical study on particle collection for wavy dielectric plate in 2-stage wire-plate electrostatic precipitator. Journal of Mechanical Science and Technology 37 (10) (2023) 5147~5157.
http://doi.org/10.1007/s12206-023-0918-3

Received December 29th, 2022
Revised April 27th, 2023
Accepted June 18th, 2023

† Recommended by Editor
Han Seo Ko

A numerical study on particle collection for wavy dielectric plate in 2-stage wire-plate electrostatic precipitator

Jae Hyun Park, Man Yeong Ha and Donggeun Lee

School of Mechanical Engineering, Pusan National University, 2 Busandaehak-ro 63beon-gil, Busan 46241, Korea

Abstract This study numerically investigated the ultrafine particle collection characteristics in the two-stage electrostatic precipitator with the dielectric plate according to the shape of the dielectric separator and air inlet velocity. This study developed a multi-physics model which analyzes the electrostatic characteristics and particle motion of the electrostatic precipitator and was implemented by using UDF (user defined function) in Ansys Fluent. The effect of the electro-hydrodynamic flow induced by the corona discharge formed in the vicinity of the high voltage wire on the air flow in the charged region of the electrostatic precipitator was investigated. The trajectories of charged ultrafine particles and their collection efficiency depended on the shape of the dielectric separator and air inlet velocity. The collection efficiency for the wavy dielectric separator is higher when the air inlet velocity is low and lower when the air inlet velocity is high, compared to that for the flat dielectric precipitator.

1. Introduction

In recent years, fine dust air pollution has become a severe environmental problem due to industrial and technological development. Fine dust particles contain various toxic substances and are harmful to human health. As a result, many countries have set regulations on ambient concentrations and emissions of particles from certain industries to address the issue of air pollution. Additionally, fine particles have been designated as carcinogens by WHO, highlighting the harmful health effects of exposure to such pollutants.

In the manufacturing process of semiconductors, battery cells, and printed circuit boards (PCBs), foreign matter management is crucial as particulates can cause product malfunction. Additionally, fine dust emissions from automobiles, factories, and industries are the primary sources of fine dust generation, leading some countries to enforce regulations. As a result, numerous researchers have been working on developing devices to reduce and eliminate fine particulate air pollutants, as described in Refs. [1-7].

An electrostatic precipitator (ESP) is a device used for removing fine dust particles and is considered an effective means for removing ultra-fine particles generated in the industrial field. It has the advantage of excellent dust collection efficiency for a range of dust particle sizes. In recent years, electric dust collection technology has been applied to remove pollutants and clean air in industrial fields, as well as indoor environments such as offices, hospitals, and homes. As the demand for stricter emission regulations of fine particles in the industrial sector and for cleaner air in the domestic environment increases, improving the performance of electrostatic precipitators becomes essential. Therefore, research is needed to identify the physical phenomena related to electrostatic precipitation.

To understand the physical phenomena in an electrostatic precipitator, it is necessary to analyze turbulent flow, behavior of ionic currents due to electrostatic fields, and particle charge and motion. The electromagnetic force generated by electric potential and ionic charge density results in an electro-hydrodynamic (EHD) flow inside the electrostatic precipitator, and the charge

density distribution affects the potential distribution due to the space charge effect. Therefore, numerical analysis techniques are being developed to simulate the electrostatic characteristics and particle behavior of electrostatic precipitators.

Cottrell [8] first invented an electrostatic precipitator that charges particles and collects the charged particles through electrostatic force. Since its invention, electrostatic precipitators have been mainly used in industrial fields to efficiently remove various fine particles. Electrostatic precipitators are widely used in industries such as cement plants, steel manufacturing facilities, coal power plants, and also in commercial and home ventilation systems. Compared to other mechanical fine particle separation devices, electrostatic precipitators can process a large amount of gas with a relatively low pressure drop and can collect various size particles very efficiently.

Mcdonald et al. [9] developed a mathematical model for electrostatic precipitator. Choi et al. [10, 11] studied a single-stage wire-plate electrostatic precipitator in which particle charging and particle collection occur simultaneously. A numerical study was conducted to identify the effect of various parameters on particle collection performance in a single-stage electrostatic precipitator. Kim et al. [12] conducted a numerical study to investigate the effect of particle size distribution on the particle collecting performance of an electrostatic precipitator. Nikas et al. [13] conducted a numerical study to figure out characteristics such as the electrostatic field distribution, fluid flow, and particle motion of a single-stage electrostatic precipitator. Lawless [14] developed a charging model considering both field charge and diffusion charge for ultra-fine particles.

Particle charging models and Lagrangian methods have been utilized by several *researchers* [15-17] to predict particle charge and motion. In this study, particle charge and motion equations were integrated over time and space. The discrete phase model (DPM) was used to model particle motion in the Lagrangian frame.

Generally, single-stage electrostatic precipitators have a simple design and are capable of collecting a large amount of dust, which makes them widely used in industries for removing large particles. However, the single-stage electrostatic precipitator has a high ozone generation rate and poor removal performance for fine and ultra-fine particles. However, the single-stage electrostatic precipitator generates much ozone and is inappropriate to remove small particles. Therefore, in residential and semiconductor fields, a two-stage electrostatic precipitator is preferred over a single-stage electrostatic precipitator.

A two-stage electrostatic precipitator operates with a lower voltage applied to the wire compared to a single-stage electrostatic precipitator. This results in a significant reduction in the amount of ozone generated by corona discharge, especially in the narrow gap between the dust collection plates. Moreover, the electric force in the collecting region of a two-stage electrostatic precipitator is stronger than that of a single-stage electrostatic precipitator. This makes it possible to remove small particles that are not strongly charged. Therefore, the two-stage electrostatic precipitator is more effective in removing fine particles.

Zhu et al. [18] conducted a study to use a two-stage wire-plate electrostatic precipitator more efficiently. They focused on improving fine particles' collection efficiency by installing a W-shaped dust collecting plate instead of a flat collecting plate.

Recently, Kim et al. [19] added a dielectric separator to the collecting region of a two-stage wire-plate electrostatic precipitator. The effect of the dielectric separator is experimentally and numerically investigated on the dust collection performance. The additional installation of the dielectric separator improved the collecting performance.

Many researchers have investigated the effect of design parameters on particle collection efficiency in a two-stage wire-plate electrostatic precipitator. However, no study has been conducted on the effect of various dielectric separator geometries of the two-stage electrostatic precipitator. Therefore, this study investigated the effect of operating conditions and type of wavy dielectric separator on the flow field and electric field distribution in a two-stage wire-plate electrostatic precipitator with a dielectric separator applied. In this study, a numerical study was conducted to figure out the particle motion according to the shape of the dielectric separator.

2. Numerical methodology

2.1 Governing equation

Fig. 1 represents the physical interaction of the electrostatic precipitator phenomenon. As shown in Fig. 1, the phenomenon occurring in the electrostatic precipitator is a multi-physics phenomenon in which the electric field, the flow field, the charge of the particles, and the motion of the particles are interlocked. In this study, ANSYS FLUENT and UDF (user defined function) were used to simulate the electric field, flow field, and particle electrification to identify multi-physics phenomena of electrostatic precipitator, and particle motion interaction. Also, the two-stage wire-plate electrostatic precipitator was considered in two dimensions.

In a two-stage electrostatic precipitator system, the air flow is described by the mass and momentum conservation equations, which are defined as follows:

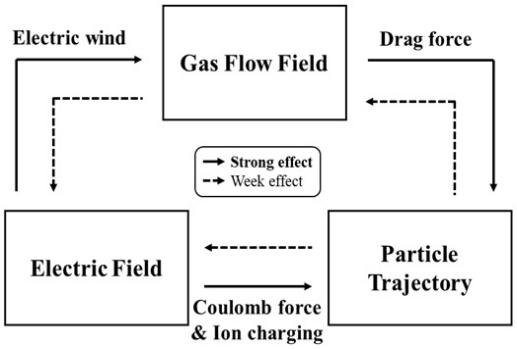

Fig. 1. Interaction of physical system in the electrostatic precipitator.

$$\frac{\partial}{\partial x_i}\left(\rho_f u_i\right)=0 \tag{1}$$

$$\frac{\partial}{\partial x_j}\left(\rho_f u_i u_j\right)=-\frac{\partial P}{\partial x_i}+\frac{\partial}{\partial x_j}\left[\mu\left(\frac{\partial u_i}{\partial x_j}+\frac{\partial u_j}{\partial x_i}\right)-\rho_f\overline{u_i' u_j'}\right]+E_i\rho_{ion}\,. \tag{2}$$

In Eq. (2), $E_i\rho_{ion}$ represents the body force of the electrostatic field on the flow field. The Reynolds stress $-\rho_f\overline{u_i' u_j'}$ was calculated using the standard k-ε turbulence model and the standard wall function model.

Corona discharge is generated by the high voltage applied to the wire. The electric potential distribution and ion field caused by corona discharge are obtained from the Poisson Eq. (3) and the charge conservation Eq. (4), as follows:

$$\frac{\partial^2\varphi}{\partial x^2{}_i}=-\frac{\rho_{ion}}{\varepsilon_0} \tag{3}$$

$$\frac{\partial}{\partial x_i}[\rho_{ion}(\mathrm{k}_{ion}E_i+u_i)-D_{ion}\frac{\partial\rho_{ion}}{\partial x_i}]=0\,. \tag{4}$$

Here E_i, ρ_{ion}, k_{ion}, D_{ion} and ε_0 represent electric field strength, ion charge density, ion mobility, ion diffusion coefficient, and permittivity of air, respectively. The electric field strength distribution E_i is obtained from Eq. (5) below.

$$E_i=-\frac{\partial\varphi}{\partial x_i}\,. \tag{5}$$

In corona discharge, there is a critical electric field strength E_{dis} that can be obtained using Peek's law defined in the equation below and is shown in Eq. (6).

$$E_{dis}=3.1\times10^6\delta(1+\frac{0.03}{\sqrt{\delta r}}) \tag{6}$$

where δ and r represents the gas relative density and the radius of the wire, respectively.

Fig. 2 shows the schematic of the collecting region in the electrostatic precipitator with the dielectric separator. A dielectric separator having a thickness b was added between the high voltage plate and ground collecting plate. If a high voltage of φ_{pl} is applied to the upper plate and the lower plate is grounded in the absence of a dielectric, a uniform electric field of field strength $E = \varphi_{pl}/d$ is obtained. In this case, the electric potential present in the dielectric separator can be defined as follows:

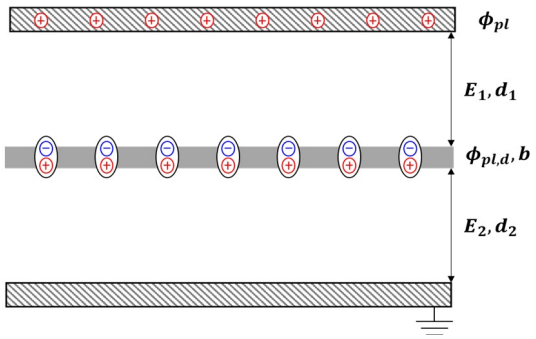

Fig. 2. Schematic of electric field formed between collection plate with dielectric plates.

$$\varphi_{pl}=d_1E_1+d_2E_2+bE_3\,. \tag{7}$$

In this study, the motion of particles was predicted using DPM (discrete phase model) method in Lagrangian frame. The particle motion equation can be expressed as follows:

$$\frac{d\vec{u}_p}{dt}=F_D(\vec{u}-\vec{u}_p)+\vec{F}_{coul}\,. \tag{8}$$

The main forces affecting the particle motion are the aerodynamic drag force and the electric force. The aerodynamic drag is defined through Eq. (9) as follows:

$$F_D=\frac{18\mu}{d_p{}^2\rho_pC_c}\,. \tag{9}$$

where μ is the kinematic viscosity coefficient of air and ρ_p is the density of particles, and C_c is the Cunningham correction coefficient, expressed as in Eq. (10).

$$C_c=1+\frac{2\lambda}{d_p}(1.257+0.4e^{-(1.1d_p/2\lambda)}) \tag{10}$$

where λ is mean free path. Also, coulomb force $\vec{F}_{coul}$ is defined as follows:

$$F_{coul}=\frac{q_pE}{m_p}=\frac{3q_pE}{4\rho_pd^3} \tag{11}$$

where q_p, m_p and ρ_p represent the charge amount of the particle, the particle mass, and the particle density, respectively.

The particle charge mechanism is divided into diffusion charge and field charge. For small particles, diffusion charging mainly operates, and for large particles, field charging mainly operates. For medium-sized particles, both charging models should be combined. In this study, we used the Lawless [9] charging model to combine field charging and diffusion charging as follows:

$$\frac{dv}{dt_q}=\begin{cases}f(w)\dfrac{v-3w}{\exp(v-3w)-1}\,, & v>3w\\[2ex] \dfrac{3w}{4}\left(1-\dfrac{v}{3w}\right)^2+f(w)\,, & -3w\le v\le 3w\\[2ex] -v+f(w)\dfrac{-v-3w}{\exp(v-3w)-1}\,, & v<-3w\end{cases} \tag{12}$$

$$f(w)=\begin{cases}\dfrac{1}{(w+0.475)^{0.575}} & ,\ w\geq 0.525\\ 1 & ,\ w<0.525\end{cases} \tag{13}$$

where $v=q_p e/2\pi\varepsilon_0 d_p k_b T$ is the dimensionless particle charge, $w=\left(K_P/K_P+2\right)\left(Ed_p e/2k_b T\right)$ is the dimensionless electric field strength, and $t_q=\rho_s k_{ion} t/\varepsilon_0$ is the dimensionless charge time. $f(w)$ is the surface area ratio corresponding to the area of diffusion charge and other regions.

Fig. 3 shows the flow chart of the electrostatic precipitator used in this study. Eqs. (1)-(7) are used to calculate the electric potential field, ionic density field, and flow field. Particle motion is then calculated using the Lagrangian method based on these fields. To calculate the electric field and ion field, particle charging, and the motion of charged particles (Eqs. (3)-(13)), UDF codes were used. The results of UDF were used to couple with the flow field and DPM to simulate the electrostatic precipitator in Fluent.

2.2 Validation

Fig. 4 shows a schematic of the electrostatic precipitator used in the experiment conducted by Parasram [20]. The diameter of the wire was 50 μm. Three wires are arranged at intervals of 50 mm at the center of the electrostatic precipitator.

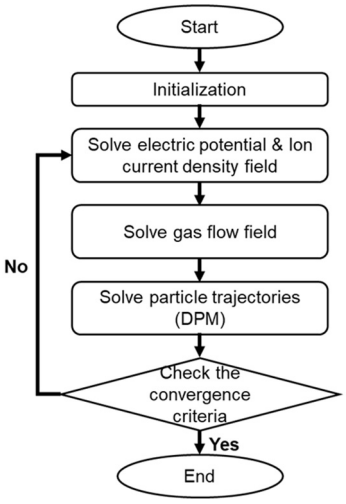

Fig. 3. Flow chart of electrostatic precipitator simulation.

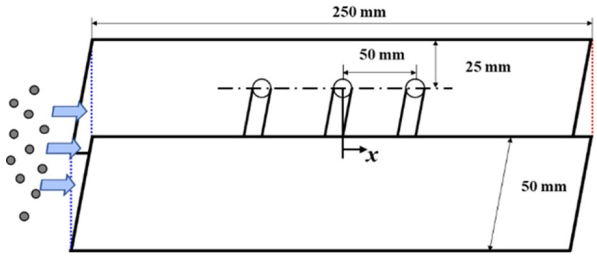

Fig. 4. Schematic of electrostatic precipitator used by Parasram [20].

The voltage applied to the wire for corona discharge was 15 kV.

Fig. 5 shows the change in current density according to the flow direction (x). To validate the numerical model developed in this study, the ion current density obtained from the present CFD simulation was compared with the value measured in the experiment of Parasram [20]. The current density distribution obtained from the present CFD simulation agrees well with the value obtained in the experiment of Parasram [20], showing the validity of the present numerical methodology used.

2.3 Computational details

Fig. 6 shows the two-dimensional electrostatic precipitator used in this study. Fig. 6(a) represents the details of electrostatic precipitator. Fig. 6(b) shows the type of dielectric separator used in this study. The numerical simulation was conducted

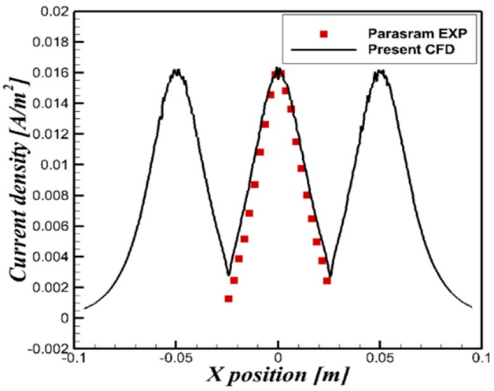

Fig. 5. Comparison of current density between the present CFD results and experiment results [20].

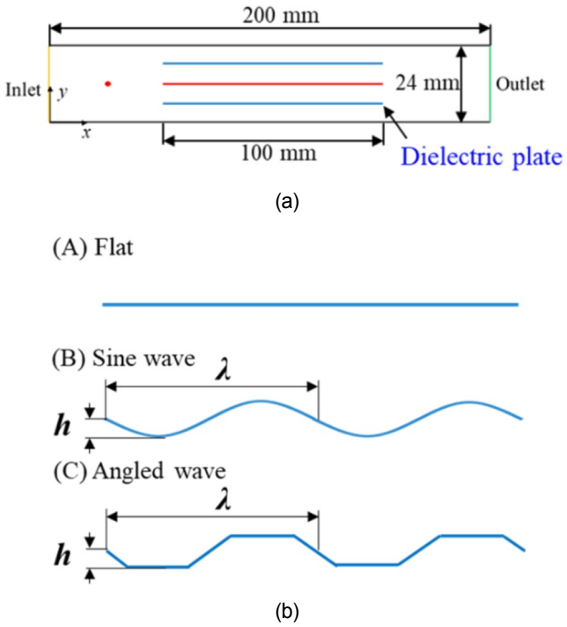

Fig. 6. Computational domain used: (a) domain details; (b) type of dielectric separator used.

by changing the shape of the dielectric separator to flat, sinusoidal and angled shapes to compare the particle collection performance. The wavy dielectric separators are h = 3 mm and λ = 50 mm. The flat dielectric separator (h = 0 mm) is the baseline case. The simulations were performed using a grid with 0.15 mm size in both the height (H) direction and airflow direction of the electrostatic precipitator. In the vertical direction in the collecting region, a 0.05 mm size grid was used so that the wall function (y+) on the surface of the collecting plate satisfies the condition of y + < 1. The total number of grids used in the electrostatic precipitator with the flat dielectric separator is 242687. In the case of using the sine wave and angled dielectric separator, 243771 and 243799 grids were used, respectively.

Table 1 shows the boundary conditions used in the present numerical analysis. In this study, the simulation was conducted while changing the air inlet velocity u_{in} from 0.45 to 1.8 m/s. In addition, Fig. 7 illustrates the number of particles, sorted by size, that were used to compare the dust collection performance of the electrostatic precipitators in this study. The calculations were performed using particles with diameters ranging between 0.3 and 1 μm. A total of 2495 particles were used for this study.

Table 1. Boundary conditions used.

Boundary	Gas flow [m/s]	Electric potential [kV]	Current density [A/m^2]
Inlet	u_{in}	0	$\frac{\partial p}{\partial n}$
Outlet	Pressure outlet	0	$\frac{\partial p}{\partial n}$
Wall duct	No slip	0	$\frac{\partial p}{\partial n}$
Wire	No slip	8.0	1.06×10^{-3}
High voltage plate	No slip	4.0	0

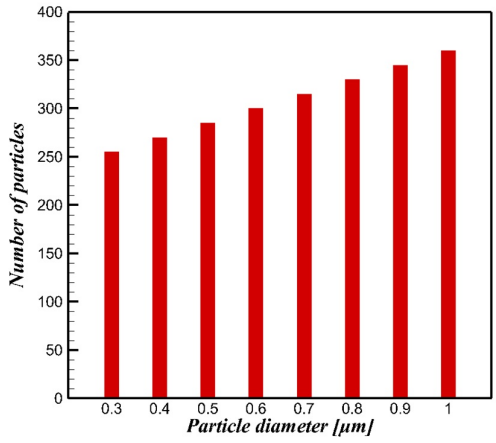

Fig. 7. Distribution of electric potential and ion density in the electrostatic precipitators with flat, sinusoidal wave and angled wave dielectric separators.

3. Numerical methodology

Fig. 8 shows the distribution of the electric potential and ion density fields for electrostatic precipitators with flat, sinusoidal and angled wavy dielectric separators. Fig. 8(a) shows the electric potential field in these precipitators with an applied voltage of 8.0 kV to the wire. The surface of the dielectric separator facing the plate connected to the high-voltage source becomes a dust-collecting plate to which the charged particles attach. This occurs due to the electric potential difference between the high voltage plate and the ground plate. So, the collecting surface area becomes larger when the dielectric separator is present than when the dielectric separator is not present. The dielectric separator's surface facing the ground collector functions to attract the charged particles towards the wall due to the dipole moment phenomenon. Fig. 8(b) shows the ion density field in electrostatic precipitators. The ion density field forms an elliptical shape around the wire and the ion current density progressively decreases as distance from the wire increases. The charging order of particles is determined by the ion current density field formed around the wire. As the charged particles pass through the collecting region, they are trapped on the plate of the collecting region due to the interaction between the electric field and the flow field.

Fig. 9 shows the distribution of air velocity fields for electrostatic precipitators with flat, sinusoidal and angled wavy dielec-

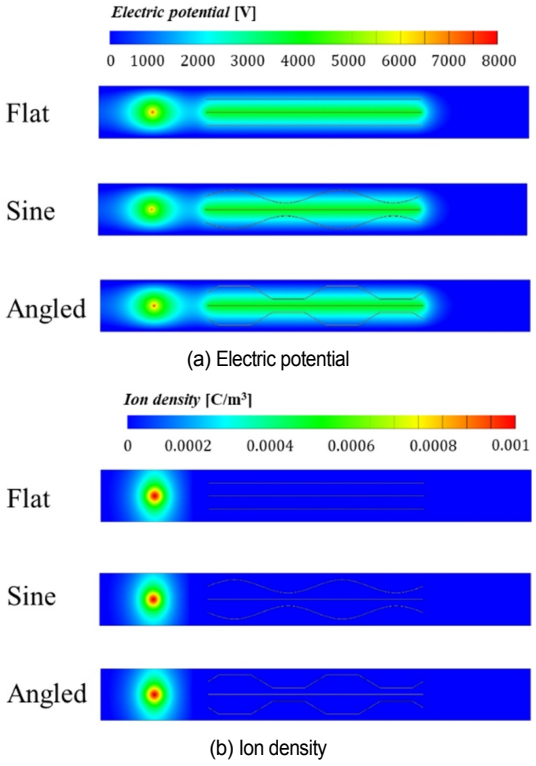

Fig. 8. Distribution of electric potential and ion density in the electrostatic precipitators with flat, sinusoidal wave and angled wave dielectric separators.

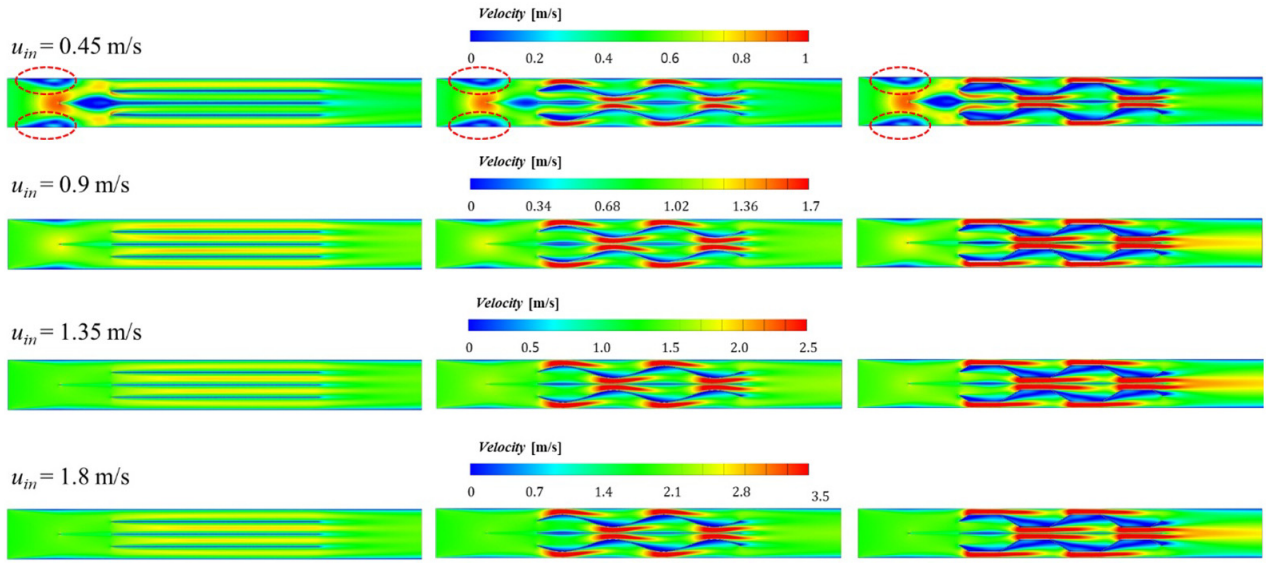

(a) Flat (b) Sine (c) Angled

Fig. 9. Distribution of air velocity fields for electrostatic precipitators with flat, sinusoidal wave and angled wave dielectric separators according to the inlet velocity.

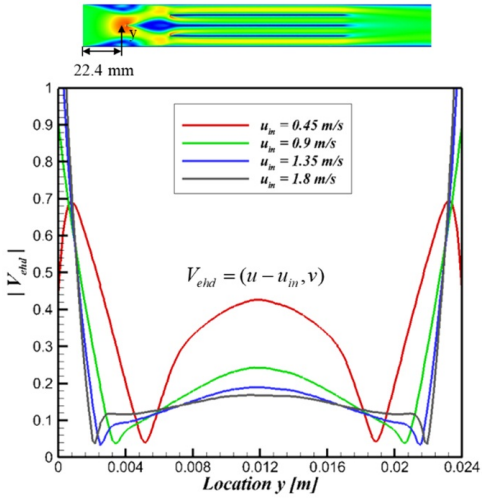

Fig. 10. EHD flow velocity magnitude at the location of x = 22.4 mm along the vertical direction for different air inlet velocities.

tric separators according to the air inlet velocity. The air flow is faster in the mountain region of the dielectric separator, and slower in the valley region. In the charged region, a wire near the inlet of the electrostatic precipitator creates a corona discharge induced electro-hydrodynamic (EHD) flow, which affects the air flow in the charged region. The EHD flow is more prominent at low inlet velocities, as shown by the red dotted line. As the inlet velocity increases, the EHD flow effect becomes less significant. The collecting region is not affected by the EHD flow.

Fig. 10 shows EHD flow velocity magnitude ($|V_{ehd}|$) at location x = 22.4mm in the charged region along the vertical y direction for different air inlet velocities. Here, $|V_{ehd}|$ is defined as follows:

$$|V_{ehd}| = \sqrt{(u - u_{in})^2 + v^2} \,. \tag{14}$$

As air flows through an electrostatic precipitator, its velocity in the x and y directions can be represented by u and v, respectively. Increasing the velocity of air entering the precipitator causes a decrease of the $|V_{ehd}|$ in the central region of the device, but an increase in velocity in the region near the wall. This phenomenon occurs due to the presence of the EHD flow in the charged region, which leads to acceleration of the air flow in the central region and formation of a recirculation zone near the wall. So, the degree to which the air flow is accelerated in the central region and the air recirculation is formed in the region near the wall in the charged region of the electrostatic precipitator is dependent on the velocity of the air inlet flow at a given voltage applied to the wire. In other words, by increasing the air inlet velocity at a given voltage, it is possible to enhance the EHD flow effect and the recirculation zone near the wall. This information can be useful in optimizing the performance of electrostatic precipitators for various industrial applications.

Fig. 11 shows the trajectories of charged ultrafine particles depending on the air inlet velocity and the shape of the collecting plate. It can be observed that, for all the cases analyzed, there is an increase in the number of particles that exit the analysis region without being captured as the air inlet velocity increases. This trend occurs because the effect of the air flow field on the motion of the particles becomes more pronounced at higher air inlet velocities. Additionally, it can be seen that as the air inlet velocity increases, the duration during which the charged particles are subject to the electric force in the collecting region decreases. These observations have important implications for the design and operation of electrostatic precipita-

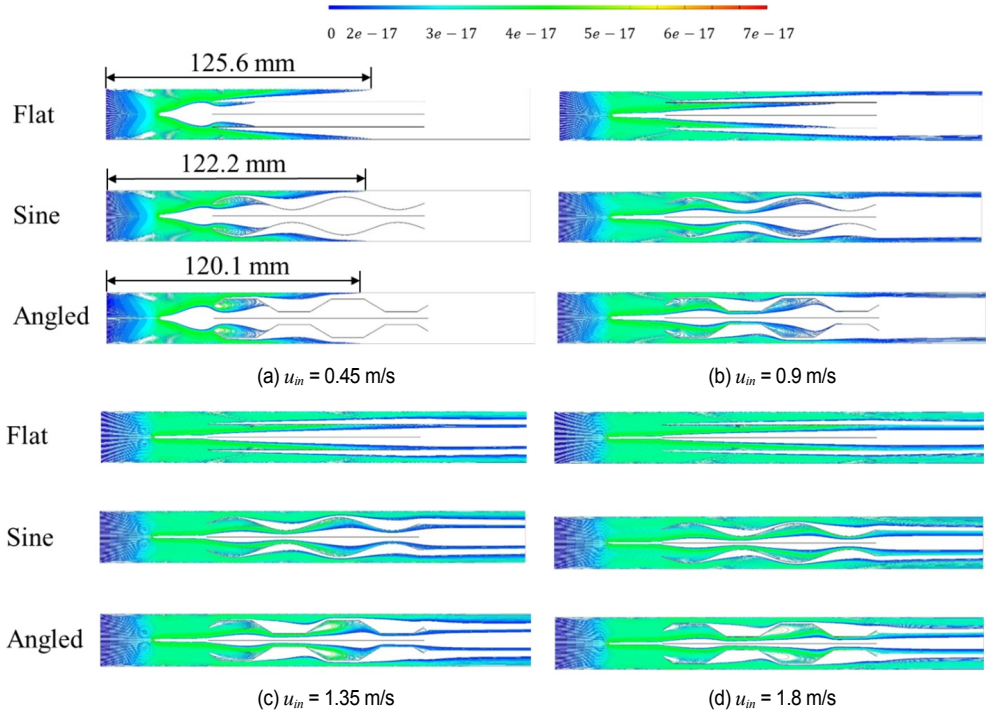

Fig. 11. Particle trajectory in the ESP for different air inlet velocities and collecting plate shapes.

tors, as they can aid in the selection of optimal air inlet velocities and collecting plate geometries to enhance particle capture efficiency.

Fig. 11(a) presents the trajectory of particles under the condition of u_{in} = 0.45 m/s. In this case, the distance traveled by particles before they are captured in the collecting region is shorter when the dielectric separator has a wavy shape compared to a flat shape. Specifically, all particles were collected within a maximum travel distance of 125.6 mm from the inlet in the baseline case with a flat dielectric separator. In contrast, when the dielectric separator had a wavy shape, all charged particles were collected within a maximum travel distance of 120.1 mm. This indicates that the maximum travel distance for particle collection with a wavy dielectric separator was reduced by approximately 4.4 % compared to the flat dielectric separator. The reason for this difference lies in the fact that as the parameter h, illustrated in Fig. 6, increases, the distance between the wavy dielectric plate and the collecting plate becomes narrower, leading to a greater likelihood of particle capture. These results demonstrate the potential for optimizing the design of electrostatic precipitators by selecting appropriate dielectric separator shapes and geometries.

Fig. 11(b) shows the particle trajectory at u_{in} = 0.9 m/s. When the air inlet velocity increases from 0.45 m/s to 0.9 m/s, some particles escape the collecting region without being captured. Therefore, we cannot directly compare the maximum travel distance for particle collection between the wavy and flat dielectric separators in this case. This means that the particle capture efficiency of electrostatic precipitators may decrease at higher air inlet velocities, and designers should carefully consider the design parameters in such situations.

Figs. 11(c) and (d) illustrate the particle trajectory at u_{in} = 1.35 m/s and 1.8 m/s, respectively. As the air inlet velocity increases, a larger number of particles exit the collecting region without being captured. This trend indicates that more particles escape through the center of the collecting region as the air inlet velocity increases.

To investigate the effect of the dielectric separator shape on the dust collection performance, the dust collection efficiency (η) is defined as follows:

$$\eta = \frac{N_{in} - N_{esc}}{N_{in}} \times 100 . \tag{15}$$

N_{in} is number of injected particles and N_{esc} is number of escaped particles without being captured on the collecting plate in the collecting region.

Fig. 12 presents the dust collection efficiency for various dielectric separator shapes at different air inlet velocities. At u_{in} = 0.45 m/s, the particles have enough residence time to be captured, resulting in a 100 % dust collection efficiency across all cases. The collection efficiency decreases almost linearly for the flat dielectric separator, but not for the wavy and angled separators, whose rate of decrease depends on the air inlet velocity. When u_{in} increases from 0.45 m/s to 0.9 m/s, the rate of decrease in efficiency for the wavy and angled separators is lower than when it increases from 0.9 m/s to 1.8 m/s, as shown in Figs. 13 and 14. Consequently, at u_{in} = 0.9 m/s, the wavy and angled dielectric separators achieve a higher collection efficiency of 97 %, compared to the 88 % efficiency of the

flat dielectric separator.

When the air inlet velocity increases from 0.9 m/s to 1.35 m/s, the decrease in collection efficiency is much more significant for the wavy and angled dielectric separators than for the flat electric separator. As a result, the difference in dust collection efficiency among the three cases considered at u_{in} = 1.35 m/s becomes very small, unlike at u_{in} = 0.9 m/s.

However, when the air inlet velocity increases to 1.8 m/s, the dust collection efficiency for each dielectric separator type is reversed, unlike at u_{in} = 0.9 m/s and u_{in} = 1.35 m/s conditions. In this case, the collection efficiency for the wavy and angled dielectric separators is lower than that for the flat dielectric separator. This is because the number of particles entering the valley region of the wavy dielectric separator decreases as the air inlet velocity increases.

Fig. 13 displays the particle trajectories in the middle of the collecting region indicated by the dotted square box of the dielectric separator for various air inlet velocities. Figs. 13(a) and (b) show the trajectories of the charged particles in the magnified area for the cases of wavy and angled dielectric separators, respectively. As the inlet velocity increases, the residence time of the particles in the collection region becomes shorter. As a result, the number of uncaptured particles increases.

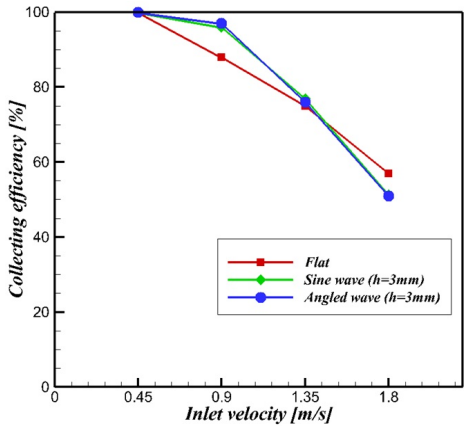

Fig. 12. Collection efficiency according to the air inlet velocity for different shapes of collecting plate.

Fig. 14 illustrates the variation in the number of particles entering and exiting the observation area in the middle of wavy and angled dielectric separators with respect to the air inlet velocity. As the air inlet velocity increases, the number of particles entering the observation area also increases, as demonstrated in Fig. 13. As the air inlet velocity increases, the number of particles not captured on the collecting plate and leaving the observation area also increases. Therefore, as the air inlet velocity increases, the ratio of the number of particles exiting to the number of particles entering the observation area also increases, indicating a gradual decrease in dust collection efficiency. Due to this reason, when u_{in} = 1.8 m/s, the dust collection efficiency of the wavy type dielectric separator is lower than that of the flat type.

Fig. 15 shows the number of particles deposited on the flat, sine and angled dielectric separators along the air flow direction for different air inlet velocities, respectively. Fig. 15(a) represents the deposited layer of particles on the flat dielectric separator. As the air inlet velocity increases, the layer of particles deposited on the dielectric separator is widely distributed and the thickness of this deposited layer of particles decreases. The position where a relatively large number of particles are collected at the given air inlet velocity is gradually located downstream as the air inlet velocity increases.

Figs. 15(b) and (c) show the deposited layer of particles on the flat dielectric separator, respectively. When u_{in} = 0.45 m/s, most of the particles are captured in the front of the dielectric separator. When u_{in} = 0.9 m/s, particles in the first valley region of the wavy dielectric separator descend downward toward the dielectric separator with relatively large residence time because of a decrease in the air velocity due to an increase in the air flow path cross-sectional area. Therefore, in

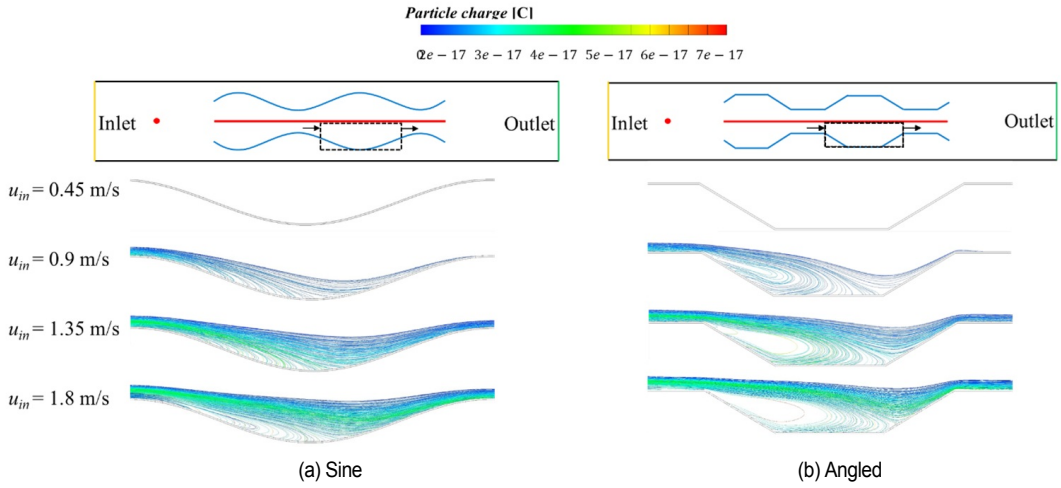

(a) Sine (b) Angled

Fig. 13. Particle trajectories in the middle of the wavy and angled dielectric separators for different air inlet velocities.

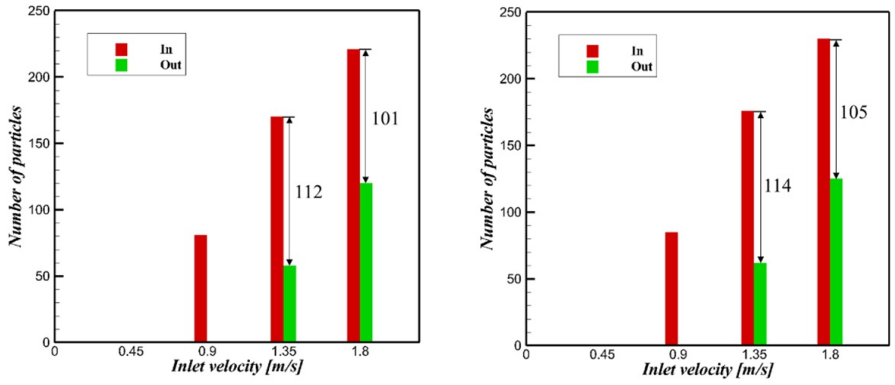

Fig. 14. Number of particles entering and exiting the area in the middle of the wave and angled dielectric separator according to the air inlet velocity.

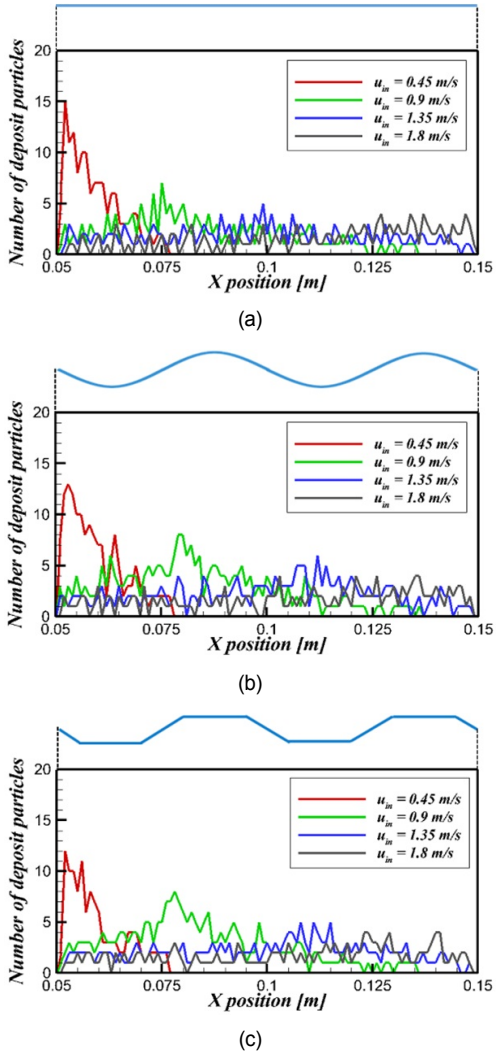

Fig. 15. Number of particles deposited on the flat, sine and angled dielectric separators along the air flow direction for different air inlet velocities.

the diverging region following the wavy dielectric separator's mountain and valley, a significant amount of particles is collected, and the number of particles deposited on the dielectric separator reaches its maximum value. When u_{in} = 1.35 m/s, many particles pass through the first valley and mountain regions without being collected due to the flow acceleration with an increase in the air inlet velocity, giving the largest number of particles deposited on the dielectric separator in the second valley region of the dielectric separator. When u_{in} = 1.8 m/s, because of high inlet air velocity, the number of particles deposited on the dielectric separator is generally smaller than that at the lower air inlet velocities of u_{in} = 0.45, 0.9 and 1.35 m/s, and as a result, the number of particles deposited on the dielectric separator has the largest value in the second mountain region of the dielectric separator.

4. Conclusions

The focus of this study was to investigate the collection efficiency of ultrafine charged particles in a two-stage wire-plate electrostatic precipitator, taking into account the shape of the dielectric separator. The study used numerical simulations to accurately represent the electro-hydrodynamic and particle motion characteristics of the precipitator. The methodology was validated by comparing the numerical results with previous experimental results.

In the charged region of the electrostatic precipitator, the strong effect of the electro-hydrodynamic flow induced by the corona discharge in the vicinity of the high voltage wire accelerates the air flow around the center while forming air flow recirculation near the wall. The impact of the EHD flow on the air flow in the charged region reduces with increasing air inlet velocity. However, in the collecting region, the air flow remains unaffected by the EHD flow.

The collection efficiency for the flat dielectric separator decreases almost linearly with increasing air inlet velocity. However, the rate of decrease in the collection efficiency for the wavy and angled dielectric separators depends on the air inlet velocity with its low and high values at the low and high air inlet velocities, respectively. This result suggests that the wavy and angled dielectric separators can be effectively used in low air velocity conditions, while the flat dielectric separator may be

more appropriate for high air velocity conditions. Therefore, the appropriate design of the dielectric separator should be selected depending on the air inlet velocity of the electrostatic precipitator system.

Acknowledgments

This research was supported by the National Research Foundation of Korea (NRF) grant funded by the Korea government (MSIT) (NRF-2019R1A5A8083201).

Nomenclature

b : Thickness of dielectric separator
C_c : Cunningham correction factor
D_{ion} : Diffusivity of ion
d_p : Particle diameter
e : Electron charge
E : Electric field strength
E_{dis} : Critical electric field strength
F_{coul} : Coulumb force per unit mass
F_D : Drag force per unit mass
g : Gravity acceleration
h : Height of wavy dielectric plate
k_b : Boltzmann constant
k_{ion} : Mobility of ion
m_p : Mass of particle
N : Number of particles
P : Pressure
q_p : Charge of particle
s : Partial length of dielectric plate
T : Temperature
t : Time
t_q : Charging time
u : Air flow velocity
u_p : Particle velocity
v : Dimensionless particle charge
w : Dimensionless electric field strength

Greek symbols

δ : Relative density
ε_0 : Air permittivity
ε_r : Particle permittivity constant
φ : Electric potential
φ_{pl} : Electric potential on plate
λ : Mean free path
η : Collecting efficiency
μ : Dynamic viscousity
ρ_f : Density of air
ρ_p : Density of particle
ρ_{ion} : Density of ion

Subscripts

d : Dielectric
esc : Escape
i, j : Tensor notation
in : Inlet

References

[1] D. Y. Pui, S. C. Chen and Z. Zuo, PM2.5 in China: measurements, sources, visibility and health effects, and mitigation, *Particuology*, 13 (2014) 1-26.
[2] K. Darcovich, K. A. Jonasson and C. E. Capes, Developments in the control of fine particulate air emissions, *Advanced Powder Technology*, 8 (3) (1997) 179-215.
[3] J. S. Shrimpton and R. I. Crane, Small electro-cyclone performance, *Chemical Engineering and Technology*, 24 (9) (1997) 951-955.
[4] X. Su, L. Zhang, Y. Xiao, M. Sun, X. Gao and J. Su, Evaluation of a flue gas cleaning system of a circulating fluidized bed incineration power plant by the analysis of pollutant emissions, *Powder Technology*, 286 (2015) 9-15.
[5] Y. Xing, F. Guo, M. Xu, X. Gui, H. Li, G. Li, Y. Xia and H. Han, Separation of unburned carbon from coal fly ash: a review, *Powder Technology*, 353 (2019) 372-384.
[6] R. W. K. Allen and A. Van Santen, Designing for pressure drop in venture scrubbers: the importance of dry pressure drop, *The Chemical Engineering Journal and the Biochemical Engineering Journal*, 61 (1996) 203-211.
[7] C. H. Huang, C. J. Tsai and Y. M. Wang, Control efficiency of submicron particles by an efficient venture scrubber system, *Journal of Environmental Engineering*, 133 (2007) 454-461.
[8] C. G. Smith and T. B. F. Cottrell, *Dry Electrostatic Precipitator*, United States Patent (2007).
[9] J. R. McDonald, W. B. Smith and H. W. Spencer III, A mathematical model for calculating electrical conditions in wire-duct electrostatic precipitation devices, *Journal of Applied Physics*, 48 (6) (1977) 2231-2243.
[10] H. Y. Choi, Y. G. Park and M. Y. Ha, Numerical study on the effect of staggered wire electrodes in an electrostatic precipitator, *Journal of Mechanical Science and Technology*, 34 (8) (2020) 3303-3310.
[11] H. Y. Choi, Y. G. Park and M. Y. Ha, Numerical simulation of the wavy collecting plate effects on the performance of an electrostatic precipitator, *Powder Technology*, 382 (2021) 232-243.
[12] S. H. Kim, H. S. Park and K. W. Lee, Theoretical model of electrostatic precipitator performance for collecting polydisperse particles, *Journal of Electrostatics*, 50 (3) (2001) 177-190.
[13] K. S. P. Nikas, A. A. Varonos and G. C. Bergeles, Numerical simulation of the flow and the collection mechanisms inside a laboratory scale electrostatic precipitator, *Journal of Electrostatics*, 63 (5) (2005) 423-443.
[14] P. A. Lawless, Particle charging bounds, symmetry relations, and an analytic charging rate model for the continuum regime, *Journal of Aerosol Science*, 27 (2) (1996) 191-215.
[15] J. H. Goo and J. W. Lee, Stochastic simulation of particle charging and collection characteristics for a wire-plate electrostatic precipitator of short length, *Journal of Aerosol Science*,

28 (5) (1997) 875-893.
[16] W. B. Smith and J. R. McDonald, Development of a theory for the charging of particles by unipolar ions, *Journal of Aerosol Science*, 7 (2) (1976) 151-166.
[17] H. J. White, Particle charging in electrostatic precipitation, *Transactions of the American Institute of Electrical Engineers*, 70 (2) (1951) 1186-1191.
[18] Y. Zhu, C. Chen, J. Shi and W. Shangguan, Enhancement of air purification by unique W-plate structure in two-stage electrostatic precipitator: A novel design for efficient capture of fine particles, *Advanced Powder Technology*, 31 (4) (2020) 1643-1648.
[19] S. Kim, K. Park, C. Choi, M. Y. Ha and D. Lee, Removal of ultrafine particles in a full-scale two-stage electrostatic precipitator employing a carbon-brush ionizer for residential use, *Building and Environment*, 223 (2022) 109493.
[20] N. Parasram, Particle motion in electric precipitators, *Ph.D Thesis*, Imperial College of Science, Technology and Medicine (2001).

Jae Hyun Park received his undergraduate degree for Mechanical Engineering at the Pusan National University, Korea, in 2021. He currently has master's degree. His research interests focus on the computational fluid dynamics.

Man Yeong Ha received his B.S. degree from Pusan National University, Korea, in 1981, M.S degree, in 1983, from Korea Advanced Institute of Science and Technology, Korea, and Ph.D. degree from Pennsylvania State University, USA in 1990. Dr. Ha is currently a Professor at the School of Mechanical Engineering at Pusan University in Busan, Korea. He serves as an Editor of the Journal of Mechanical Science and Technology. His research interests are focused on thermal management, computational fluid dynamics, and micro/nano fluidics.

Donggeun Lee is a Professor at School of Mechanical Engineering, Pusan National University. He received his B.S. degree, M.S. degree, and Ph.D. degree from Seoul National University in 1994, 1996, and 2000, respectively. He serves as an editor of Advanced Powder Technology and as an advisory board member of Aerosol Science and Technology. His life-long research interest was in aerosol science dealing with particulate matters suspended in gas (or liquid). Now, he has focused on dry cleaning of 10nm particulate contaminants on Si wafer using sub- or super-critical CO2 fluid, and understanding ions' and nanoparticles' behaviors in ESP-based residential air purifying systems.